

**Nuclear transparency in quasielastic $A(e, e'p)$:
intranuclear cascade versus eikonal approximation**

Ye.S. Golubeva

Institute of Nuclear Research, 117312 Moscow, Russia

L.A. Kondratyuk

Institute of Theoretical and Experimental Physics, 117259 Moscow, Russia

A. Bianconi

Dipartimento di Chimica e Fisica per i Materiali e per l'Ingegneria,

Università di Brescia, I-25133 Brescia, Italy,

and Istituto Nazionale di Fisica Nucleare, Sezione di Pavia, I-27100 Pavia, Italy

S. Boffi and M. Radici

Dipartimento di Fisica Nucleare e Teorica, Università di Pavia,

and Istituto Nazionale di Fisica Nucleare, Sezione di Pavia, I-27100 Pavia, Italy

(October 3, 2018)

Abstract

The problem of nucleon propagation through the nuclear medium in quasielastic $A(e, e'p)$ reactions is discussed in the kinematic range $1 \leq Q^2 \leq 7$ $(\text{GeV}/c)^2$. Experimental data are available from SLAC, BATES and, recently, also from TJNAF. The coefficient of nuclear transparency is calculated for each Q^2 in the framework of the intranuclear cascade model (INC) and of the eikonal approximation (EA). The former has the capability of directly implementing the detector acceptances giving a very detailed analysis of the

different observables. The latter, essentially based on an exclusive mechanism, contains explicit information about the dependence on the target shell structure. The predictions of both models are in good agreement with each other. The INC model reproduces the experimental data quite well in the measured range. The EA gives an explanation of the Q^2 behaviour of the transparency coefficient as a kinematic effect related to the superposition of contributions from each target shell.

25.30.Rw, 24.10.Eq, 11.80.Fv, 24.60.Gv .

I. INTRODUCTION

The issue of nucleon propagation through the nuclear medium as a major problem in understanding nuclear reactions has received much attention during the last decades. The best tool of investigation is probably given by an electromagnetic probe knocking out a nucleon from the nucleus A , such as in $A(e, e'p)$ reactions under quasielastic kinematic conditions [1,2]. In this case, the whole nuclear volume is explored, the elementary electron-proton scattering cross section is well known, and high resolution experiments allow for a clean detection of ejected protons under several kinematic conditions.

At intermediate energies much work has been done, both theoretically and experimentally (see, e.g., Ref. [3] for a review), and final-state interactions (FSI) of the ejected proton with the residual $A - 1$ system seem to be well described by an optical potential within the distorted-wave impulse approximation (DWIA). For large enough $Q^2 = q^2 - \omega^2$, where ω and \mathbf{q} are the energy and momentum transferred by the electron to the target, respectively, perturbative QCD predicts the so-called phenomenon of color transparency [4–6], i.e. for increasing Q^2 the struck hadron should propagate undergoing a decreasing interaction with the nuclear environment. Consequently, the detected proton would emerge under conditions asymptotically approaching the predictions of the plane-wave impulse approximation (PWIA) (see Refs. [7–9] for a review).

Experiments have been performed recently at SLAC [10,11] and TJNAF [12]. The SLAC data have been taken in the range $1 \leq Q^2 \leq 7$ (GeV/c)² and their Q^2 and A dependence do not show conclusive evidence that the transparency increases with Q^2 . The new data from TJNAF at $0.64 \leq Q^2 \leq 3.3$ (GeV/c)² are in reasonable agreement with the prior data from SLAC. A variety of models have been proposed to describe either the evolution of color neutral and compact hadron configurations leading to color transparency [4–6,13–18], or the nuclear transparency of proton propagation using conventional degrees of freedom in the Glauber model [19–21]. The data do not rule out the possibility of a slow onset of color transparency, but conventional explanations of nuclear transparency (NT) have to be first

investigated in detail. In fact, this has been done in Ref. [11] within the classical Glauber model and the effective nucleon-nucleon (NN) total cross section in nuclear medium σ_{eff} has been found lower than the free one σ_{free} by $\sim 30\%$. Some reduction of the NN cross section in nuclear medium is indeed expected from Pauli blocking and short-range correlations [22] as well as from quantum interference between coherent and incoherent rescatterings [19–21].

The aim of this paper is twofold. We shall first try to study the NT occurring during the motion of the ejected proton in terms of a quasiclassical solution of the multiple scattering. Our approach will adopt the intranuclear cascade model (INC), a model successfully developed for the description of hadron-nucleus collisions at intermediate energies [23,24] and recently extended [25–27] to account for the in-medium effects in the production of vector mesons on nuclei. Then, the results will be compared with experimental data and with the predictions of the standard eikonal approximation (EA) [28], which has been tested and shown to give results for exclusive $A(e, e'p)$ reactions at $0.8 \leq Q^2 \leq 4$ (GeV/c)² in remarkable agreement, over a wide range of proton angles, with the predictions based on the well established optical potential approach [29–31].

In Sec. II the INC model is applied to quasielastic semi-inclusive $A(e, e'p)$ reactions. After a brief presentation of the model in Sec. II A, momentum and angular PWIA distributions of the final electrons and protons at different Q^2 and for different targets are generated in Sec. II B taking advantage of the model capability to give a very detailed analysis of different observables with direct inclusion of detector acceptances, in contrast to more conventional analytical approaches. The effects of FSI are discussed in Sec. II C. In Sec. III a brief review of EA is presented together with a definition of NT suitable for comparison with a semi-inclusive measurement. The theoretical cross section, essentially based on an exclusive mechanism, takes into account only the channels related to the direct proton knockout. However, unlike other semi-inclusive calculations [19–21], it contains explicitly a detailed information on the target shell structure. Results of the INC model are compared with data and with the EA prediction in Sec. IV. Some conclusions are presented in Sec. V.

II. QUASIELASTIC $A(e, e'p)$ WITHIN THE FRAMEWORK OF INC

In the following, a general description of the INC model is given and angular and energy distributions of generated events are discussed for the quasielastic semi-inclusive $A(e, e'p)$ reaction on several nuclei.

A. The INC model

The INC model was originally applied to the analysis of hadron-nucleus interactions [23,24]. It can be considered as a quasiclassical numerical representation of the multiple scattering series. It differs from the standard Glauber approximation [28] in the description of the multiple incoherent scattering terms. In the latter, with the so-called frozen approximation, the motion of the scattering centers is neglected, while the INC model takes it into account explicitly.

Within the INC framework the linearized kinetic equation for the many-body distribution function, describing hadron transport in nuclear matter [32], is solved numerically by assuming that during the evolution of the cascade the properties of the target nucleus remain unchanged. This implies that the number of cascade particles N_c is much less than the number of nucleons A in the target nucleus. In the case of light nuclei this condition might be violated at proton momenta larger than 5 GeV/ c , where events with large multiplicities could be overestimated. This condition does not prevent the application of the INC model to the description of SLAC [10,11] and TJNAF [12] data.

Another feature of the INC model is the fact that the model is quasiclassical. This might appear a limitation because, consequently, it cannot describe genuine quantum effects such as the coherent rescattering. If those effects would be important in the case of quasielastic $A(e, e'p)$ reactions the application of the INC model would be doubtful. The struck nucleon, after receiving a large Q^2 , can in principle scatter on the residual system in a coherent and incoherent way. However, in practice in the present kinematic conditions it cannot transfer a

small momentum to the recoiling system because of Pauli blocking. Therefore, the coherent rescattering is expected to be suppressed, and incoherent rescattering can adequately be described by the INC model. On the contrary, within the conventional Glauber approximation the coherent rescattering is usually overestimated, because its probability is the same as for the incoherent one and its weight is determined by the free NN total cross section.

Within the INC model the target nucleus is regarded as a mixture of degenerate neutron and proton Fermi gases in a spherical potential well with a diffuse surface. The momentum distribution of the nucleons is treated in the local density approximation for a Fermi gas. The nucleus is divided into a series of concentric zones which help to follow the propagation of each produced particle from one zone to another. At the beginning of the cascade a large sample of struck nucleons is generated. It corresponds to the kinematic conditions of the quasielastic peak, when the energy E_e of the initial electron and Q^2 are fixed by the experiment. In this case the scattering angle for free elastic electron-proton scattering is also fixed. The momentum and angular distributions of final electrons and struck protons, created in any given zone, are determined by the Fermi momentum distributions in the same zone. If necessary, final cuts in the momentum and angular distributions can be applied according to experimental acceptances. The relative numbers of struck nucleons produced in different zones are proportional to the local densities.

The model describes in a straightforward way the development of the cascade when the struck proton rescatters elastically or produces any number of additional particles, such as pions. Between different collisions the particles propagate along straight-line trajectories and the location of the next collision is generated assuming a weight function exponentially decreasing with the propagation distance. At each step of the cascade, the competition among different channels is governed by the channel cross sections, which are taken as in vacuum apart from the effect of the Pauli exclusion principle taken into account at each collision. This means that rescattering may occur only when the momentum of each recoiling nucleon is out of the Fermi sphere. In other words, the damping of the ejectile flux along its trajectory is determined not by the free NN total cross section, but by a smaller effective cross

section due to Pauli blocking. In principle, the number of protons counted in the detector includes also those created with different momenta and subsequently modified by rescattering and eventually appeared within the momentum acceptance of the detector. These events, which correspond to many-fold elastic rescattering, are also taken into account by the INC mechanism.

Masses, energies and momentum components for all the particles in the initial, final and any intermediate step of the cascade, are recorded for every event and any necessary distribution involving those quantities can be produced.

B. Momentum and angular distributions in PWIA

In Figs. 1-3 momentum and angular distributions in the kinematic conditions of the NE18 experiment [10] for carbon are shown for events generated without FSI, i.e. in PWIA. In all figures the solid line refers to $Q^2 = 1.04 \text{ (GeV}/c)^2$, $E_e = 2.015 \text{ GeV}$ and the dashed line to $Q^2 = 6.77 \text{ (GeV}/c)^2$, $E_e = 5.12 \text{ GeV}$, respectively.

In Fig. 1a at $Q^2 = 1.04 \text{ (GeV}/c)^2$ the momentum distribution $N(p_e)$ of electrons is strongly peaked around $1.5 \text{ (GeV}/c)^2$, while at $Q^2 = 6.77 \text{ (GeV}/c)^2$ it is much broader and extends over a range of roughly $2 \text{ GeV}/c$. The main reason for this broadening is that at higher electron energies the spreading of the c.m. energy due to Fermi motion is much more pronounced. In Fig. 1b the momentum distributions $N(p')$ of final protons are presented. Their shapes are qualitatively similar to those for electrons, They have, however, different positions of the maxima.

The angular distributions of final electrons ($N(\theta_e)$) and protons ($N(\theta_p)$) are shown in Figs. 2a and 2b, respectively. The angle θ_e is the scattering angle, while θ_p is defined in the electron scattering plane with respect to a \hat{z} axis directed along the incident beam. The INC model reproduces the expected spread of the angular distributions due to Fermi motion.

The angular distribution $N(\phi_{ep})$ is shown in Fig. 3 for events corresponding to protons ejected out of the scattering plane. In fact, ϕ_{ep} is the angle between the electron scattering

plane and the plane defined by the momenta \mathbf{p}' and \mathbf{p}_e of the emitted proton and the incident electron, respectively. If Fermi motion would be absent, this distribution in the c.m. of the final system would be described by the delta function $\delta(\phi_{ep} - \pi)$. On the contrary, the width of this distribution is determined by the ratio between the transverse component of the Fermi momentum with respect to the scattering plane and \mathbf{p}' . At larger Q^2 , p' is larger and the distribution becomes narrower.

C. The effect of FSI

Fig. 4 shows the proton spectrum $N(p')$ integrated over the angles θ_p and ϕ_{ep} at $Q^2 = 1.04$ (GeV/c)², $E_e = 2.015$ GeV in PWIA (dashed line) and with FSI computed within the INC model (solid line). In the upper part (Fig. 4a) the protons are emitted from carbon; therefore, the dashed line corresponds to the solid line in Fig. 1b on a smaller scale. As expected, the struck proton loses part of its momentum because of rescattering and pion production. Consequently, FSI make the spectrum softer and move part of the strength to lower momenta. The effect is even more pronounced for gold (Fig. 4b).

In a very similar manner, the same effect is evident also for the angular distributions of final protons scattered in plane ($N(\theta_p)$) and out of plane ($N(\phi_{ep})$), as it is shown in Fig. 5a and Fig. 5b, respectively, for carbon and gold targets in the same conditions and with the same notations as in Fig. 4, except that the distribution is integrated over the interval $1.1 \leq p' \leq 1.3$ GeV/c. In this case, FSI redistribute the events over a wider angular range because of rescattering.

Experimental setups usually require kinematic cuts on momentum, angular and missing momentum/energy distributions. Therefore, it is important to compare those distributions in cases where FSI are switched off and on for the same cuts. This can be done in the INC model in a natural way.

The solid circles in Fig. 5 describe the ratio $T_{\text{INC}} = N_{\text{FSI}}/N_{\text{PWIA}}$ between the distributions of events with and without FSI, that is actually equivalent to NT. In the range of angles

around the maximum, the ratio T_{INC} , integrated over the other variables, is approximately constant. For example, integrating over ϕ_{ep} for carbon $T_{\text{INC}} \sim 0.6 \div 0.7$ for $34^\circ \leq \theta_p \leq 54^\circ$ and for gold $T_{\text{INC}} \sim 0.25 \div 0.35$ for $34^\circ \leq \theta_p \leq 56^\circ$. Similarly, integrating over θ_p T_{INC} gets the same values for carbon and gold, respectively, in the range $165^\circ \leq \phi_{ep} \leq 195^\circ$.

This stability of T_{INC} over rather wide angular intervals suggests that it depends mainly on the nuclear density along the propagation trajectory of the struck proton. If the angular cuts would be performed inside the above indicated intervals, the size of T_{INC} would be almost independent of the specific choice of the cuts. As the angular distributions N_{INC} are broader than N_{PWIA} , the values of T_{INC} increase in the tail regions and have a large uncertainty at those angles, where the proton yield, calculated in PWIA, is very small and the dominant contribution comes from rescattering.

The version of the INC model here adopted cannot give completely realistic distributions in missing momentum ($\mathbf{p}_m = \mathbf{p}' - \mathbf{q}$) and missing energy (E_m), because it uses a spectral function corresponding to the Fermi gas model. However it is instructive to analyse the p_m dependence of the ratio T_{INC} in comparison with the one of the conventional Glauber approach.

In Ref. [20] it is argued that, after integrating over the missing momentum p_{m_T} transverse to the propagation axis, only the inelastic proton-nucleon cross section should contribute to the Glauber multiple-scattering series, which describes the attenuation of the ejected proton flux. The argument is that the elastic cross section leads just to a broadening of the p_{m_T} distribution while inelastic rescatterings suppress the ejectile flux at any p_{m_T} , according to a mechanism similar to the Gribov's inelastic shadowing [33]. Since at $p_{m_T} = 0$ the total proton-nucleon cross section contributes, in this framework NT is expected to be an increasing function with p_{m_T} .

In Fig. 6a and Fig. 6b the missing momentum distributions for carbon and gold targets are shown, respectively, at the same Q^2, E_e and with the same notations as in Fig. 4. The sign of p_m , according to Ref. [12], is defined positive (negative) when the angle of \mathbf{p}' with respect to the incident beam is larger (smaller) than the angle of \mathbf{q} . The general trend

is that, at least at relatively small outgoing proton angles, T_{INC} decreases with increasing $|p_m|$ (and, therefore, $|p_{m_T}|$), contrary to the previous expectations and in agreement with Ref. [30] (see, in particular, Fig. 4 therein at angles corresponding to p_m below the Fermi momentum). A possible explanation (confirmed and justified also in the framework of the EA, see Sec. IV) relies on the observation that struck protons with higher missing momenta mainly come from deeper zones inside the nucleus. Therefore they must propagate through larger distances inside the nuclear medium before escaping towards the detector.

Imposing a constraint on the range of explored missing momenta, as in the NE18 experiment [11] where $0 \leq p_m \leq 250 \text{ MeV}/c$, could affect the previous argument based on the interference between elastic and inelastic channels. A quantitative estimate is possible in the INC model, where all particles can be tagged and recognized at each step during their propagation inside the nuclear medium. Therefore, one can compute the number N_{dir} of events obtained according to the attenuation of the proton flux in the forward direction and the number N_{resc} of events where the protons fell into the detector acceptance coming from very different initial conditions due to elastic and inelastic rescatterings. Two conditions were selected that correspond to $Q^2 = 1.04$ and $6.77 \text{ (GeV}/c)^2$ in the NE18 experiment [11], but no cuts were applied on p_m (see Table I). The kinematic restrictions for p' and ϕ_{ep} are slightly softer than in the NE18 experiment [11], but further checks at points with higher statistics have shown that the results are stable against stronger cuts. As indicated in Table I, the ratio $R = N_{\text{resc}}/N_{\text{dir}}$ is always small. Therefore, under the conditions of the NE18 experiment [11] the fraction of indirect protons reaching the detector with large p_{m_T} after elastic or inelastic rescattering is small.

III. NUCLEAR TRANSPARENCY IN EA

In exclusive $(e, e'p)$ reactions on nuclei, where the residual system is left in a well defined final state, the basic ingredient of the calculation is the scattering amplitude [2]

$$J_{\alpha}^{\mu}(Q^2, \mathbf{q}, E_{R_{\alpha}}) = \int d\mathbf{r} d\sigma e^{i\mathbf{q}\cdot\mathbf{r}} \chi_{\mathbf{p}'}^{(-)*}(\mathbf{r}, \sigma) \hat{J}^{\mu}(Q^2, \mathbf{q}, \mathbf{r}, \sigma) \phi_{\alpha, E_{R_{\alpha}}}(\mathbf{r}, \sigma), \quad (1)$$

where \hat{J}^μ is the nuclear charge-current density operator. The scattering wave function $\chi_{\mathbf{p}'}^{(-)}$ is the solution of a Schrödinger equation involving an optical potential V which effectively describes the interaction between the residual nucleus, recoiling with momentum $-\mathbf{p}_m$ and mass M_R , and the outgoing proton, detected in the direction defined by $\cos \gamma = \mathbf{p}' \cdot \mathbf{q}/p'q$. The proton bound state $\phi_{\alpha, E_{R_\alpha}}$ is the solution of an eigenvalue problem involving a single-particle local potential of the Woods-Saxon type, which also depends on the excitation energy E_{R_α} of the residual nucleus corresponding to the proton removal from the shell with quantum numbers α . Since the kinetic energy of the residual nucleus is given by [1,3]

$$K_{R_\alpha} = \left(p_m^2 + (M_R + E_{R_\alpha})^2 \right)^{1/2} - M_R - E_{R_\alpha}, \quad (2)$$

also the missing energy of the reaction explicitly depends on the produced hole through the relation

$$E_{m_\alpha} = \omega - K_{p'} - K_{R_\alpha}. \quad (3)$$

Therefore, in the following, the complete dependence of the scattering amplitude on the bound-state quantum numbers α is exploited by the notation $J_\alpha^\mu(Q^2, \mathbf{p}_m, E_{m_\alpha})$.

Here our interest is on the properties of the scattering wave $\chi_{\mathbf{p}'}^{(-)}$ and the simplified picture is considered retaining just the longitudinal component \hat{J}^0 to leading order $o(1)$ of the nonrelativistic expansion. Consequently, the cross section becomes proportional to [29–31]

$$\left| \int d\mathbf{r} d\sigma e^{i\mathbf{q}\cdot\mathbf{r}} \chi_{\mathbf{p}'}^{(-)*}(\mathbf{r}, \sigma) \phi_{\alpha, E_{R_\alpha}}(\mathbf{r}, \sigma) \right|^2 \equiv S_\alpha^D(Q^2, \mathbf{p}_m, E_{m_\alpha}), \quad (4)$$

which is traditionally identified as the “distorted” spectral density S_α^D [34] at the missing energy E_{m_α} of the residual nucleus with a hole with quantum numbers α .

The Schrödinger equation for the scattering state can be solved for each partial wave of $\chi_{\mathbf{p}'}^{(-)}$ up to a maximum angular momentum $L_{\max}(p')$, which satisfies a convergence criterion. The boundary condition is such that each incoming partial wave coincides asymptotically with the corresponding component of the plane wave associated to p' . Typically, this method has been successfully applied to $(e, e'p)$ scattering with proton momenta below 0.5 GeV/c

and $L_{\max} < 50$ for a large variety of complex optical potentials, including also spin degrees of freedom [3].

At higher energies the Glauber method [28] suggests an alternative way (based on the EA) to solve the Schrödinger equation by reducing it to a first-order differential equation along the propagation axis \hat{z} :

$$\left(\frac{\partial}{\partial z} - ip'\right)\chi = \frac{1}{2ip'}V\chi. \quad (5)$$

The standard boundary condition requires that asymptotically $\chi \rightarrow 1$ corresponding to an incoming unitary flux of plane waves. By substituting the solution of Eq. (5) into Eq. (4) one gets the final expression for the distorted spectral density [31]:

$$S_{\alpha}^D(Q^2, \mathbf{p}_m, E_{m_{\alpha}}) = \left| \int d\mathbf{r} \phi_{\alpha, E_{R\alpha}}(\mathbf{r}, \sigma) \times \exp\left(-i\mathbf{p}_m \cdot \mathbf{r} + \int_z^{+\infty} V(\mathbf{r}_{\perp}, z') dz'\right) \right|^2. \quad (6)$$

In the pure Glauber model $V(r)$ is determined in a parameter-free way starting from the elementary free proton-nucleon scattering amplitudes at the considered energy, while at lower energies, for $(e, e'p)$ reactions under quasi-elastic conditions, it usually has a Woods-Saxon form whose parameters are fixed by fitting the phase-shifts and the analysing power of elastic (inelastic) (p, p) scattering on the corresponding residual nucleus [3].

The EA, whose reliability is supposed to increase with increasing ejectile energy [28], has been successfully tested [29–31] in the momentum range of interest here ($1 \leq p' \leq 6$ GeV/c) against the solution of the Schrödinger equation up to $L_{\max} = 120$, as required by the mentioned convergence criterion. We adopt here the same simple Woods-Saxon form for the potential $V(r)$, i.e.

$$V(r) = (U + iW) \frac{1}{1 + e^{(r-R)/a}} \equiv (U + iW) \rho(r), \quad (7)$$

where $\rho(r)$ is normalized such that $\rho(0) = 1$, a is the nuclear diffuseness and $R = 1.2 \times A^{1/3}$ fm.

At the considered proton momenta, the elementary proton-nucleon scattering amplitude is dominated by inelastic processes and $V(r)$ is supposed to be mostly sensitive to the imaginary well depth W [35]. However, no phenomenological phase-shift analysis is available

beyond the inelastic threshold, which could constrain U and W . It has been shown elsewhere [30,31] that S_α^D is rather clearly insensitive to the sign and magnitude of U for different test values of (U, W) , which justifies the choice $U = 0$, also here adopted. This choice does not contradict the Glauber model, where the ratio U/W should equal the ratio between the real and the imaginary parts of the average proton-nucleon forward-scattering amplitude, because this ratio is expected to be small anyway above the inelastic threshold [35].

As suggested by Eq. (5), the Glauber approach predicts $W \propto p'$ as far as the proton-nucleon total cross section (and, consequently, the damping of the proton flux) can be considered constant for different choices of $\mathbf{p}' \simeq \mathbf{q}$, i.e. for small angles γ . However, in order to reproduce the NE18 data [11], a smaller proportionality factor W/p' seems to be required with respect to the one indicated by the Glauber model [22,19,36,37]. Here, we adopt the choice $W = 50 p'/1400$ MeV which reproduces the damping, observed in the NE18 experiment for ^{12}C at $p' \simeq q = 1.4$ GeV/ c [10]. This choice is equivalent to retaining the full Glauber method, but assuming a smaller proton-nucleon cross section in nuclear matter than in free space [31].

In order to compare the SLAC data with a theoretical prediction based on the $S_\alpha^D(Q^2, \mathbf{p}_m, E_{m_\alpha})$ of Eq. (6), which explicitly depends on the quantum numbers α of the produced hole and, therefore, refers to a completely exclusive process, it is necessary to define a theoretical NT coefficient as follows:

$$T_{\text{EA}}(Q^2) = \frac{\sum_\alpha \sum_{p_m} S_\alpha^D(Q^2, \mathbf{p}_m, E_{m_\alpha})}{\sum_\alpha \sum_{p_m} S_\alpha^{PW}(Q^2, \mathbf{p}_m, E_{m_\alpha})}. \quad (8)$$

Eq. (8) gives the ratio between the nuclear responses S_α^D and S_α^{PW} obtained with and without FSI, respectively, for each Q^2 incoherently summed over the range of proton angles γ covered by the NE18 experiment (corresponding to different p_m [11]) and over the quantum numbers α of the occupied shells in the considered target nucleus.

IV. COMPARISON WITH DATA

Experimental data for NT in quasielastic $A(e, e'p)$ reactions are available from BATES [38], SLAC [10,11] and, in a preliminar form, from TJNAF [12]. They are obtained by taking the ratio between the sum over the observed events in the selected kinematic region and the corresponding theoretical quantity calculated in PWIA for the same region, except for the BATES experiment where the ratio between exclusive and inclusive cross sections was taken. The data cover the range $0.3 \leq Q^2 \lesssim 7 \text{ (GeV}/c)^2$.

In Fig. 7 open symbols refer to the NE18 experiment performed at SLAC, with the exception of the point at $Q^2 \sim 0.3 \text{ (GeV}/c)^2$ that has been obtained at BATES. Solid symbols indicate the preliminar data from TJNAF. From top to bottom, circles, squares and triangles give the results for carbon, iron and gold targets, respectively. Theoretical calculations of T_{INC} in the framework of the INC model are indicated by solid lines. They implement all the experimental cuts in angles and momenta as well as the integration over missing momenta and energies covered by the NE18 experiment [10,11]. Agreement with data is quite satisfactory and is confirmed in Fig. 8, where the A dependence of T_{INC} , integrated over missing momentum and energy, is shown for fixed values of Q^2 .

For sake of comparison, in Fig. 7 the dashed line shows the result of T_{EA} obtained for carbon after summing over its occupied $s_{\frac{1}{2}}$ and $p_{\frac{3}{2}}$ shells in Eq. (8) as well as over p_m in the range corresponding to the proton angles measured in the NE18 experiment [10]. In fact, in the fixed kinematics of an exclusive reaction there is a one-to-one correspondence between p_m and θ_p (or, equivalently, γ). Agreement with data is very good. Also the similarity between the results of two completely different models is remarkable.

This is confirmed in Fig. 9, where the comparison between the INC model and the EA is extended also to the ^{40}Ca target. The shape of T_{EA} (indicated by the dashed line) is essentially given by the fact that, according to the NE18 experimental setup, for each Q^2 different ranges are covered for the proton angles, and consequently for the missing momentum p_m . The different shells, then, contribute differently with their p_m dependence

so that at each Q^2 , according to the selected range of p_m , the relative weight of their contribution is changing. As a test, in Fig. 9 the dot-dashed line is also shown, which refers to NT for the $^{40}\text{Ca}(e, e'p)$ reaction in the same kinematics of the NE18 experiment but keeping the outgoing proton angle $\gamma = 0$ at each value of Q^2 : keeping the same proton angle makes NT independent of Q^2 , at least in the observed range.

The exclusive nature of direct knockout, intrinsic in the definition of T_{EA} in Eq. (8), allows for a more detailed analysis of the contribution of each shell to the integrated transparency as well as to its angular distribution. In Fig. 10a (upper part) the PWIA nuclear response S_{α}^{PW} , obtained from Eq. (6) without FSI, is shown as a function of the proton angle γ for the $^{40}\text{Ca}(e, e'p)$ reaction at $p' = q = 1 \text{ GeV}/c$. The labels refer to the quantum numbers of the shells building up the structure of ^{40}Ca . At very forward angles protons only come from s shells. At higher angles the $2s\frac{1}{2}$ contribution is irrelevant and protons with a non negligible p_{m_T} come from p and d orbitals, as well as from $1s\frac{1}{2}$. In Fig. 10b (lower part) the corresponding NT calculated in the EA framework is shown for each shell as a function of γ in the same conditions. The curve labelled by “tot” refers to the angular distribution of the total transparency for the ^{40}Ca target. The angular dependence of the total NT is determined by the dominant contribution of the individual shells at each specific angle. Therefore, at low angles the total result is due to a delicate interplay between $2s\frac{1}{2}$ and $1s\frac{1}{2}$ shells, whose transparencies are very different. At higher angles, the total result approximately follows the NT of the p and d orbitals. Globally, the total NT is a decreasing function of γ , or, equivalently, of p_{m_T} , in agreement with the findings of Sec. II C described in Fig. 6. The same arguments apply to Fig. 11, where the angular range explores the same range of p_m as in Fig. 10, but at $p' = q = 6 \text{ GeV}/c$. The NT property of being a decreasing function of p_{m_T} is even more evident. Large variations of NT with the proton emission angle γ are then possible. The larger Q^2 and p' , the smaller is the γ corresponding to the same p_{m_T} . Therefore, within the experimental acceptance (2°) [10] the corresponding angular averaging could miss significant variations of NT.

In both Figs. 10 and 11 the p and d angular distributions do not start from $\gamma = 0$,

because the PWIA result is vanishing and, therefore, not contributing to the T_{EA} of Eq. (8), while producing an artificial infinity in the transparency of the single shell at that angle.

Finally, comparison of Figs. 10b and 11b shows that integrating over γ the curves labelled by “tot” (therefore, integrating them over the same range of p_m reached at different Q^2) will produce the same total NT coefficient, in agreement with the dot-dashed line of Fig. 9. Therefore, as previously anticipated, the Q^2 dependence shown by solid and dashed lines in Fig. 9 and by data in Fig. 7 can be interpreted, in the framework of the EA, as a kinematic effect related to the shell structure of the target. At different Q^2 , probing different p_m means probing different relative weights of each shell contributing to the total NT; FSI will be less (more) effective producing an increasing (decreasing) transparency.

V. CONCLUSIONS

Nuclear transparency in exclusive quasielastic $A(e, e'p)$ reactions has been investigated. Final-state interactions have been treated within the intranuclear cascade model and the eikonal approximation. The INC model describes the available data on NT up to $Q^2 \sim 7$ GeV²/c² rather well without the need of free parameters. Our analysis shows that the Pauli blocking seems to be the most crucial ingredient and suppresses the otherwise important interference between coherent and incoherent rescatterings [19–21], while short-range correlations at such Q^2 are less important. The results of the INC model are also in qualitative agreement with those obtained in the EA.

In this framework, the Q^2 behaviour of NT can be interpreted as a kinematic effect related to the fact that for each Q^2 different ranges of missing proton momentum are explored according to the experimental setup. In fact, because in the EA the definition of NT is based on a genuine exclusive cross section, at each Q^2 it is possible to analyse the angular distribution not only of NT, but also of the contribution of each single target shell. It turns out that NT at small proton angles is due to the emission from s shells, while at larger angles shells with higher angular momentum are important. The different FSI make

NT a decreasing function of the proton angle (or, equivalently, of the transverse missing momentum p_{m_T}) and large variations of the NT coefficient are possible within the presently available experimental angular acceptance. The relative angular contribution of each shell depends on p_{m_T} . If the range of explored p_{m_T} is kept constant, the transparency coefficient, integrated over the proton angles, does not show any Q^2 dependence.

In the kinematic conditions presently investigated nuclear transparency seems under control. In order to test the onset of other transparency mechanisms as a function of Q^2 , our analysis shows that it is important to keep constant the range of missing momenta covered by the experiments.

ACKNOWLEDGMENTS

Two of us (Ye. G. and L.A. K.) are grateful to Dipartimento di Fisica Nucleare e Teorica of the University of Pavia for kind hospitality. This work was supported by INFN (Italy), by the International Association for the Promotion of Cooperation with Scientists from the Independent States of the Former Soviet Union (grant no. INTAS-93-79 Ext.) and performed in part under the contract ERB FMRX-CT-96-0008 within the frame of the Training and Mobility of Researchers Programme of the Commission of the European Union.

REFERENCES

- [1] S. Frullani and J. Mougey, *Adv. Nucl. Phys.* **13**, 1 (1984).
- [2] S. Boffi, C. Giusti, and F. D. Pacati, *Phys. Rep.* **226**, 1 (1993).
- [3] S. Boffi, C. Giusti, F. D. Pacati, and M. Radici, *Electromagnetic Response of Atomic Nuclei*, Vol. 20 of *Oxford Studies in Nuclear Physics* (Oxford University Press, Oxford, 1996).
- [4] S. J. Brodsky, in *Proceedings of the XIII International Symposium on Multiparticle Dynamics*, edited by W. Kittel, W. Metzger, and A. Stergiou (World Scientific, Singapore, 1982), p. 963.
- [5] A. H. Mueller, in *Proceedings of the XVII Rencontre de Moriond*, edited by J. Tran Thanh Van (Editions Frontières, Gif-sur-Yvette, 1982), p. 13.
- [6] S. J. Brodsky and A. H. Mueller, *Phys. Lett.* **B206**, 685 (1988).
- [7] L. L. Frankfurt, G. A. Miller, and M. I. Strikman, *Annu. Rev. Nucl. Part. Sci.* **45**, 501 (1994).
- [8] N. N. Nikolaev, *Int. J. Mod. Phys.* **E3**, 1 (1994).
- [9] A. Bianconi, S. Boffi, and D. E. Kharzeev, *Yad. Fiz.* **57**, 1732 (1994).
- [10] N. C. R. Makins *et al.* (the NE18 Collaboration), *Phys. Rev. Lett.* **72**, 1986 (1994).
- [11] T. G. O'Neill *et al.* (the NE18 Collaboration), *Phys. Lett.* **B351**, 87 (1995).
- [12] D. Potterveld *et al.*, in *Proceedings of the Conference on Perspectives in Hadronic Physics*, edited by S. Boffi, C. C. degli Atti, and M. M. Giannini (World Scientific, Singapore, in press).
- [13] G. R. Farrar, H. Liu, L. L. Frankfurt, and M. I. Strikman, *Phys. Rev. Lett.* **61**, 686 (1988).

- [14] B. K. Jennings and G. A. Miller, Phys. Rev. **D44**, 692 (1991).
- [15] O. Benhar *et al.*, Phys. Rev. **C44**, 2328 (1991).
- [16] L. L. Frankfurt, G. A. Miller, and M. I. Strikman, Comm. Nucl. Part. Phys. **21**, 1 (1992).
- [17] N. N. Nikolaev, Comm. Nucl. Part. Phys. **21**, 41 (1992).
- [18] N. N. Nikolaev *et al.*, Nucl. Phys. **A567**, 781 (1994).
- [19] N. N. Nikolaev *et al.*, Phys. Rev. **C50**, R1296 (1994).
- [20] N. N. Nikolaev *et al.*, Nucl. Phys. **A582**, 665 (1995).
- [21] N. N. Nikolaev, J. Speth, and B. G. Zakharov, ZhETF **109**, 1948 (1996).
- [22] V. R. Pandharipande and S. C. Pieper, Phys. Rev. **C45**, 791 (1992).
- [23] Y. S. Golubeva, A. S. Iljinov, B. V. Krippa, and I. A. Pshenichnov, Nucl. Phys. **A537**, 393 (1992).
- [24] A. S. Botvina, Y. S. Golubeva, A. S. Iljinov, and I. A. Pshenichnov, Yad. Fiz. **55**, 1323 (1992).
- [25] Y. S. Golubeva, A. S. Iljinov, and L. A. Kondratyuk, Phys. of Atomic Nuclei **59**, 1894 (1996).
- [26] W. Cassing, Y. S. Golubeva, A. S. Iljinov, and L. A. Kondratyuk, Phys. Lett. **B396**, 26 (1997).
- [27] Y. S. Golubeva, L. A. Kondratyuk, and W. Cassing, Nucl. Phys. **A**, (to be published).
- [28] R. J. Glauber, in *Lectures in Theoretical Physics*, edited by W. Brittain and L. G. Dunham (Interscience Publ., New York, 1959), Vol. 1.
- [29] A. Bianconi and M. Radici, Phys. Lett. **B363**, 24 (1995).

- [30] A. Bianconi and M. Radici, Phys. Rev. **C53**, R563 (1996).
- [31] A. Bianconi and M. Radici, Phys. Rev. **C54**, 3117 (1996).
- [32] V. E. Bunakov, Russ. J. of Part. and Nuclei **11**, 1285 (1980).
- [33] N. N. Nikolaev and V. I. Zakharov, Phys. Lett. **B55**, 397 (1975).
- [34] S. Boffi, C. Giusti, F. D. Pacati, and S. Frullani, Nucl. Phys. **A319**, 461 (1979).
- [35] C. Lechanoine-Leluc and F. Lehar, Rev. Mod. Phys. **65**, 47 (1993).
- [36] A. Kohama, K. Yazaki, and R. Seki, Nucl. Phys. **A536**, 716 (1992).
- [37] L. L. Frankfurt, E. J. Moniz, M. M. Sargsyan, and M. I. Strikman, Phys. Rev. **C51**, 3435 (1995).
- [38] G. Garino *et al.*, Phys. Rev. **C45**, 780 (1992).

FIGURES

FIG. 1. Momentum distributions of events generated by the INC model in PWIA for final electrons (a) and protons (b) in the $^{12}\text{C}(e, e'p)$ reaction in the kinematics of the NE18 experiment. Solid lines refer to $Q^2 = 1.04 \text{ (GeV}/c)^2$, $E_e = 2.015 \text{ GeV}$, and dashed lines to $Q^2 = 6.77 \text{ (GeV}/c)^2$, $E_e = 5.12 \text{ GeV}$, respectively.

FIG. 2. Angular distributions of events generated by the INC model in PWIA for final electrons (a) and protons (b) in the electron scattering plane and in the same conditions and notations as in Fig. 1.

FIG. 3. Angular distributions of out-of-plane events generated by the INC model in PWIA as a function of the angle ϕ_{ep} between the electron scattering plane and the plane defined by the proton and beam momenta. Kinematics and notations as in Fig. 1.

FIG. 4. Proton momentum distributions, integrated over the angles θ_p and ϕ_{ep} (see text), for the $(e, e'p)$ reaction on C (a) and Au (b) at $Q^2 = 1.04 \text{ (GeV}/c)^2$, $E_e = 2.015 \text{ GeV}$. The solid and dashed lines are results of the INC model with and without FSI, respectively.

FIG. 5. Angular distributions, integrated over the proton momentum interval $1.1 - 1.3 \text{ GeV}/c$, for protons detected in the scattering plane (a) and out of plane (b) in the $(e, e'p)$ reaction on C (left) and Au (right) at $Q^2 = 1.04 \text{ (GeV}/c)^2$, $E_e = 2.015 \text{ GeV}$, with the same notations as in Fig. 4. The solid circles are the ratio between the results given by the solid and dashed lines, that is equivalent to the nuclear transparency coefficient (see text).

FIG. 6. Proton missing momentum distributions and nuclear transparency coefficient generated by the INC model in the $(e, e'p)$ reaction on C (a) and Au (b) at $Q^2 = 1.04 \text{ (GeV}/c)^2$, $E_e = 2.015 \text{ GeV}$, with the same notations as in Fig. 4.

FIG. 7. Nuclear transparency, integrated over missing momentum and energy, as a function of Q^2 for the $A(e, e'p)$ reaction. Open symbols are data from the NE18 experiment at SLAC, but for the point at $Q^2 = 0.3 \text{ (GeV}/c)^2$ obtained at BATES. Solid symbols are the preliminar data taken at TJNAF. Circles, squares and triangles refer to carbon, iron and gold targets, respectively. The solid lines are results of the INC model, while the dashed line is obtained in the EA for carbon.

FIG. 8. Nuclear transparency, integrated over missing momentum and energy, as a function of A and Q^2 . Data are from the NE18 experiment at SLAC. The solid lines are the result from the INC model.

FIG. 9. Nuclear transparency, integrated over missing momentum and energy, as a function of Q^2 for the $A(e, e'p)$ reaction on ^{12}C and ^{40}Ca targets. The solid and dashed lines are results of the INC model and of the EA, respectively. The dot-dashed line is the result of the EA for ^{40}Ca with $\gamma = 0$ at all values of Q^2 (see text).

FIG. 10. Angular distributions of the PWIA nuclear response (a) and of the nuclear transparency calculated in the EA framework (b) of each target shell for the $^{40}\text{Ca}(e, e'p)$ reaction at $p' = q = 1 \text{ GeV}/c$. The resulting total nuclear transparency of Eq. (8) is also plotted in the lower part (b) and labelled “tot”.

FIG. 11. The same as in Fig. 10 but for $p' = q = 6 \text{ GeV}/c$.

TABLES

TABLE I. The ratio $R = N_{\text{resc}}/N_{\text{dir}}$ between events for rescattered (N_{resc}) and directly attenuated (N_{dir}) protons for the $A(e, e'p)$ reaction on C, Fe and Au targets in the kinematics of the NE18 experiment but without cuts on p_m (see text).

Q^2 (GeV/c) ²	θ_e deg	p' GeV/c	θ_p deg	ϕ_{ep} deg	R
1.04	32-39	1.1-1.3	40-53	170-190	2.6 % (C), 4.2 % (Fe), 5.7 % (Au)
6.77	56.1-57.1	4.4-4.6	15.5-17.5	170-190	≤ 0.4 %

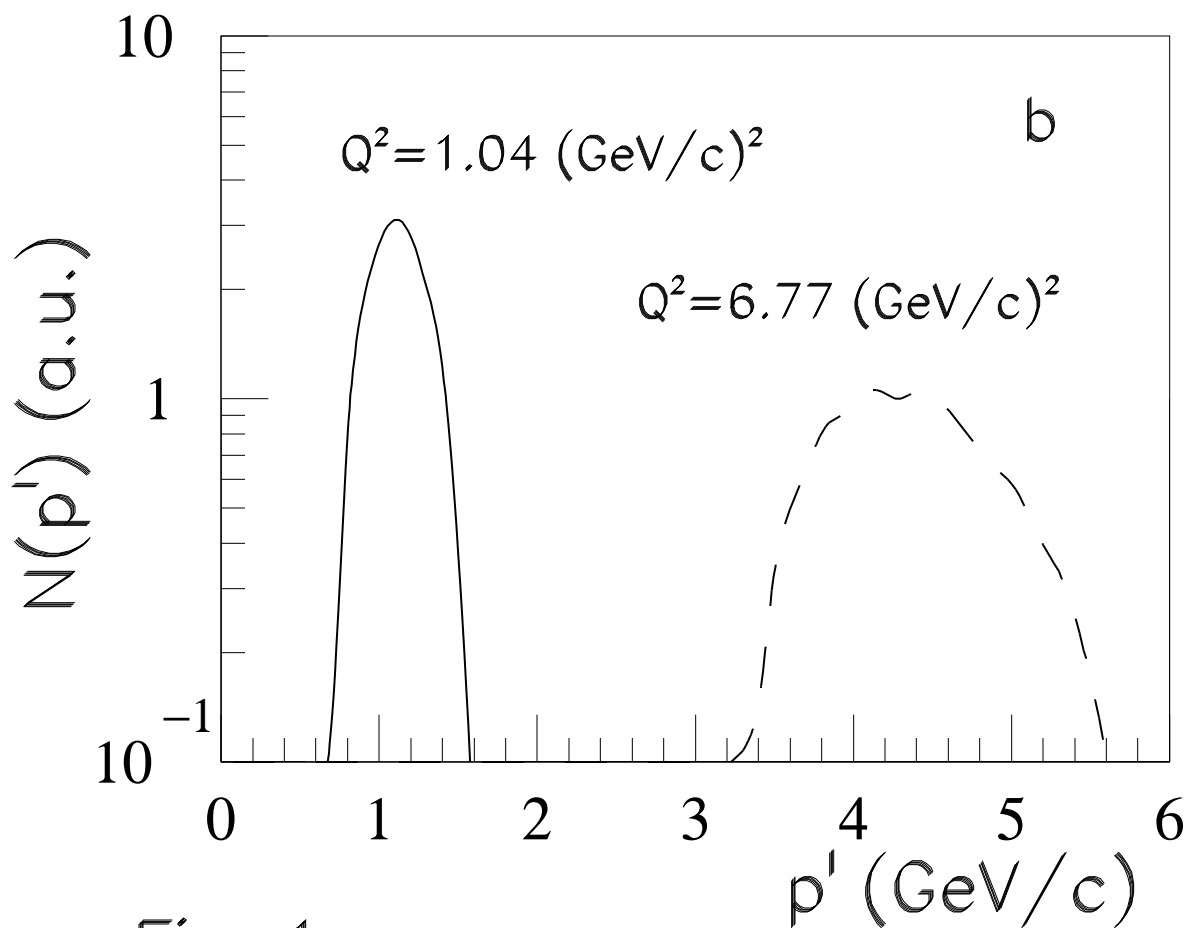
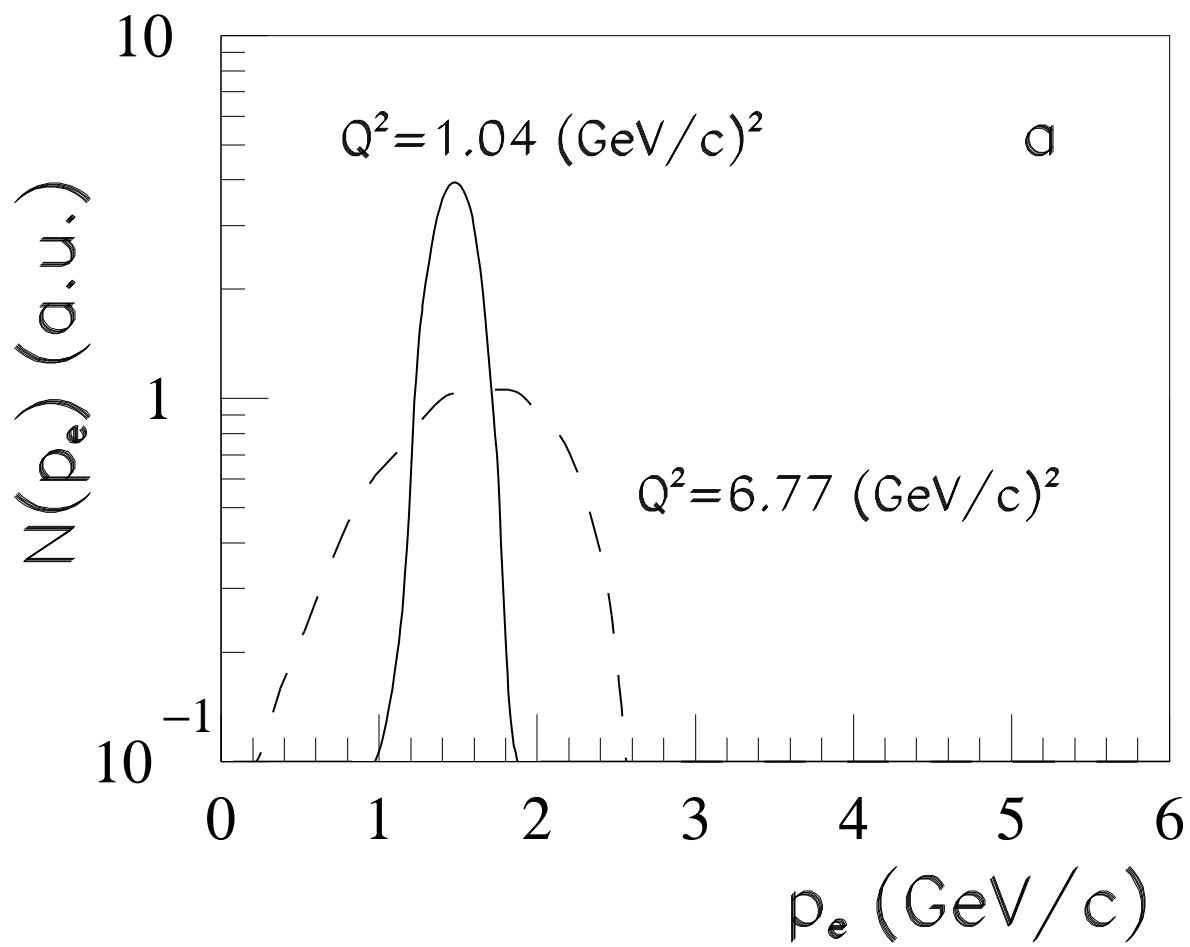


Fig. 1

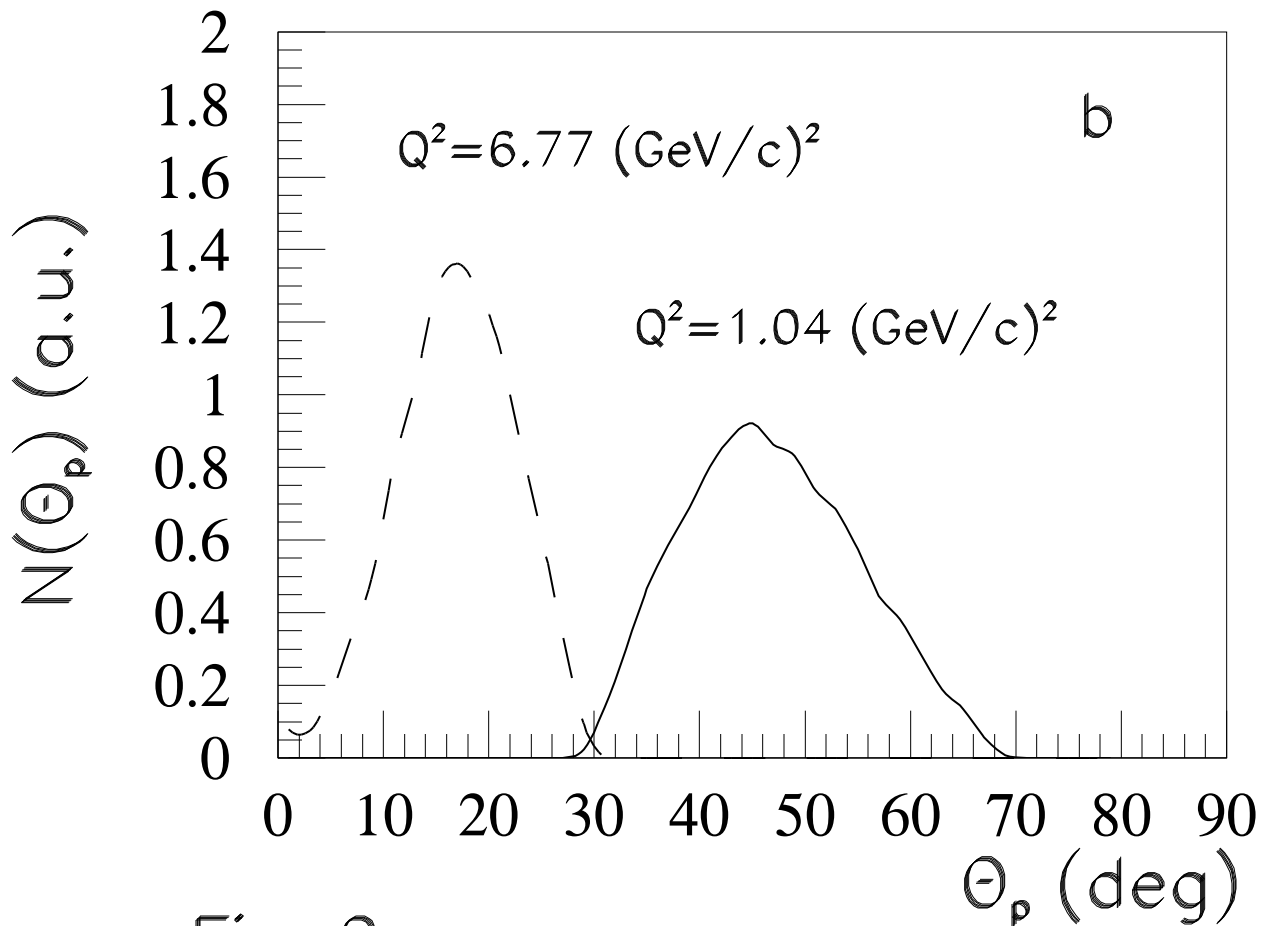
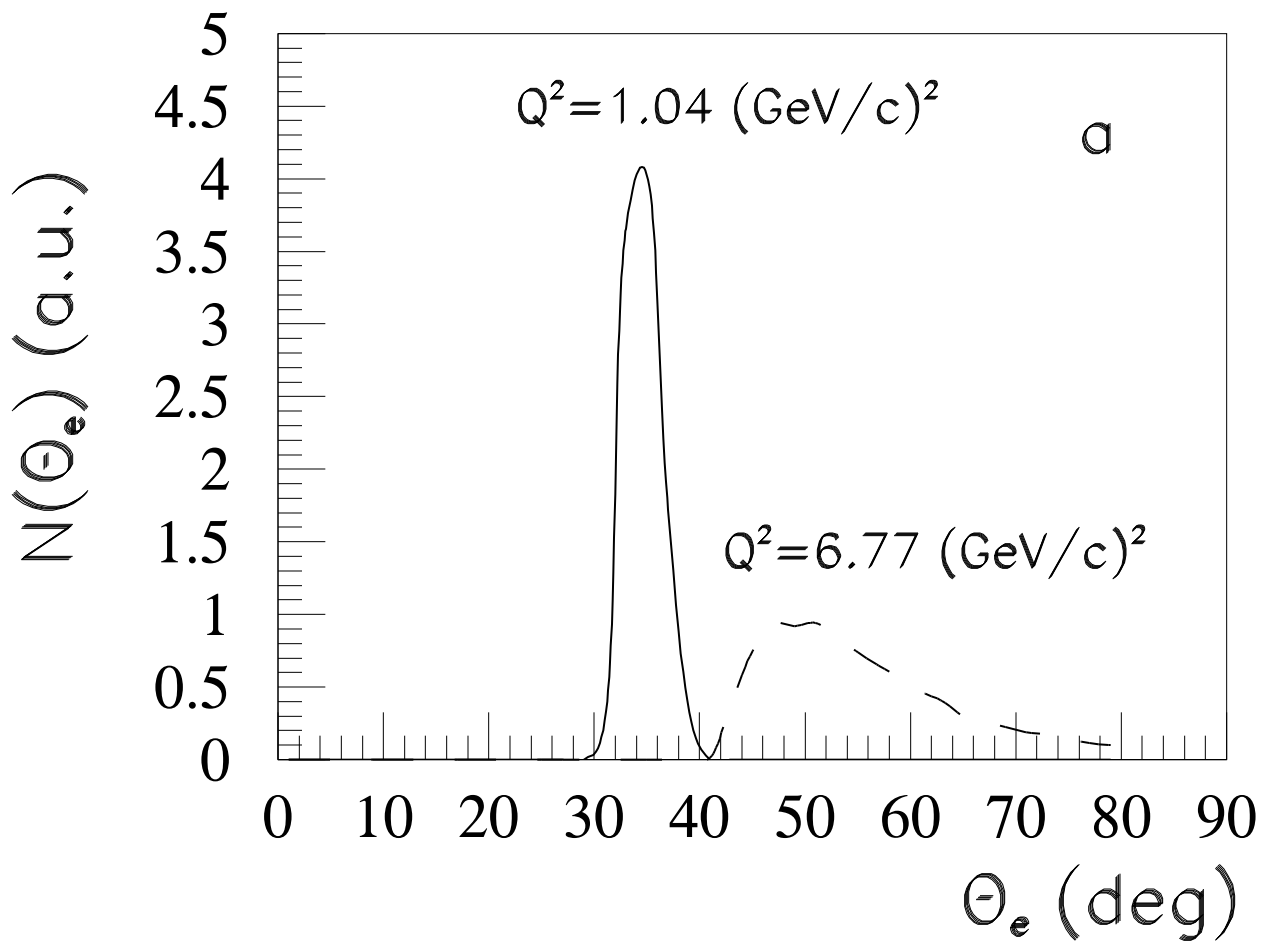


Fig. 2

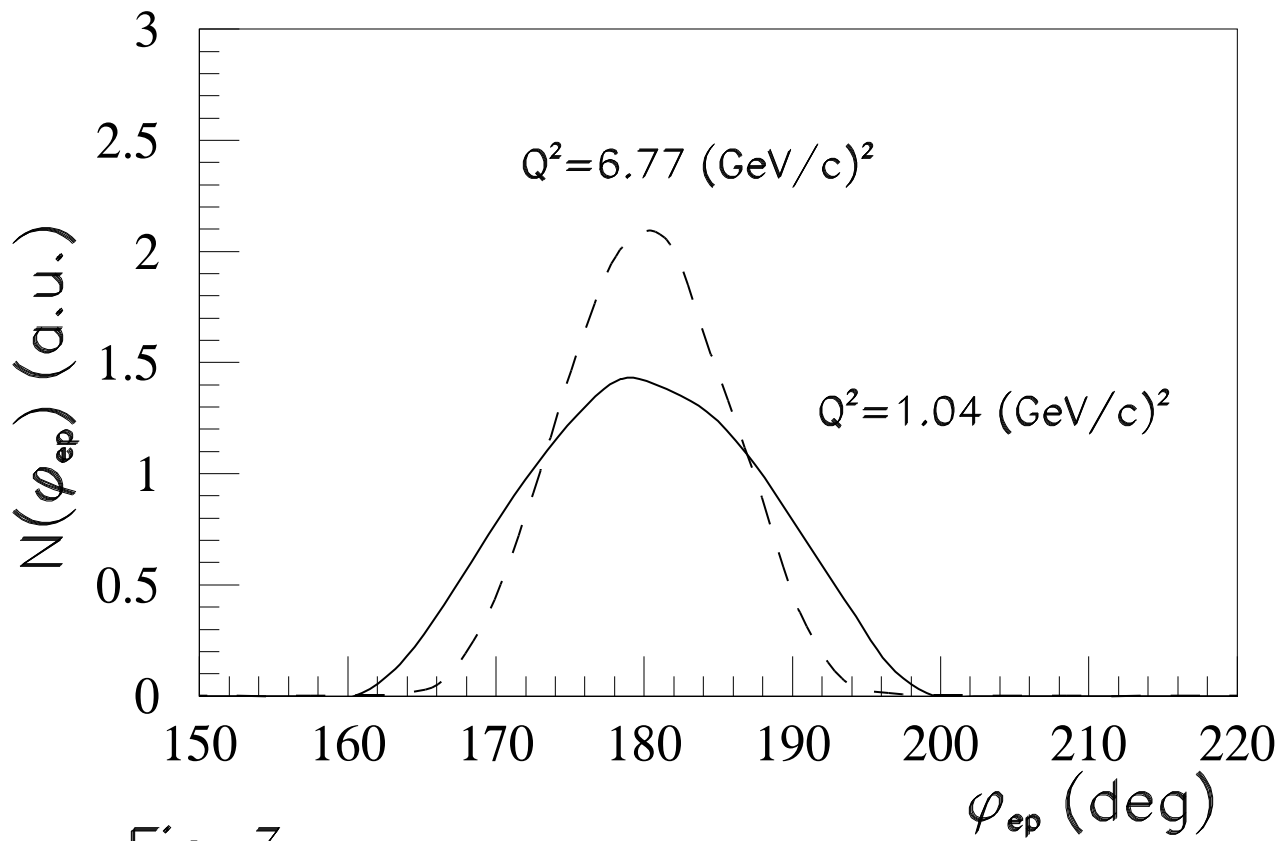


Fig. 3

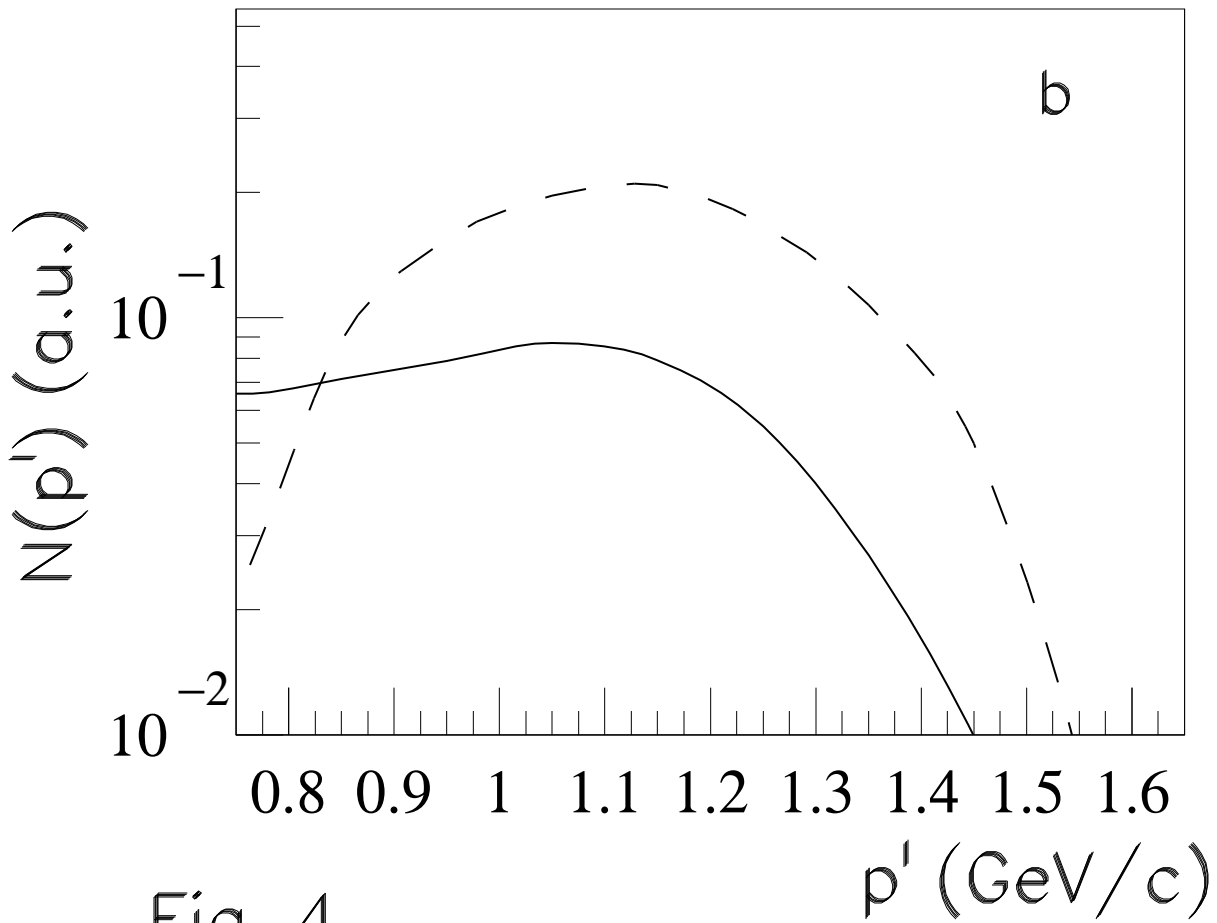
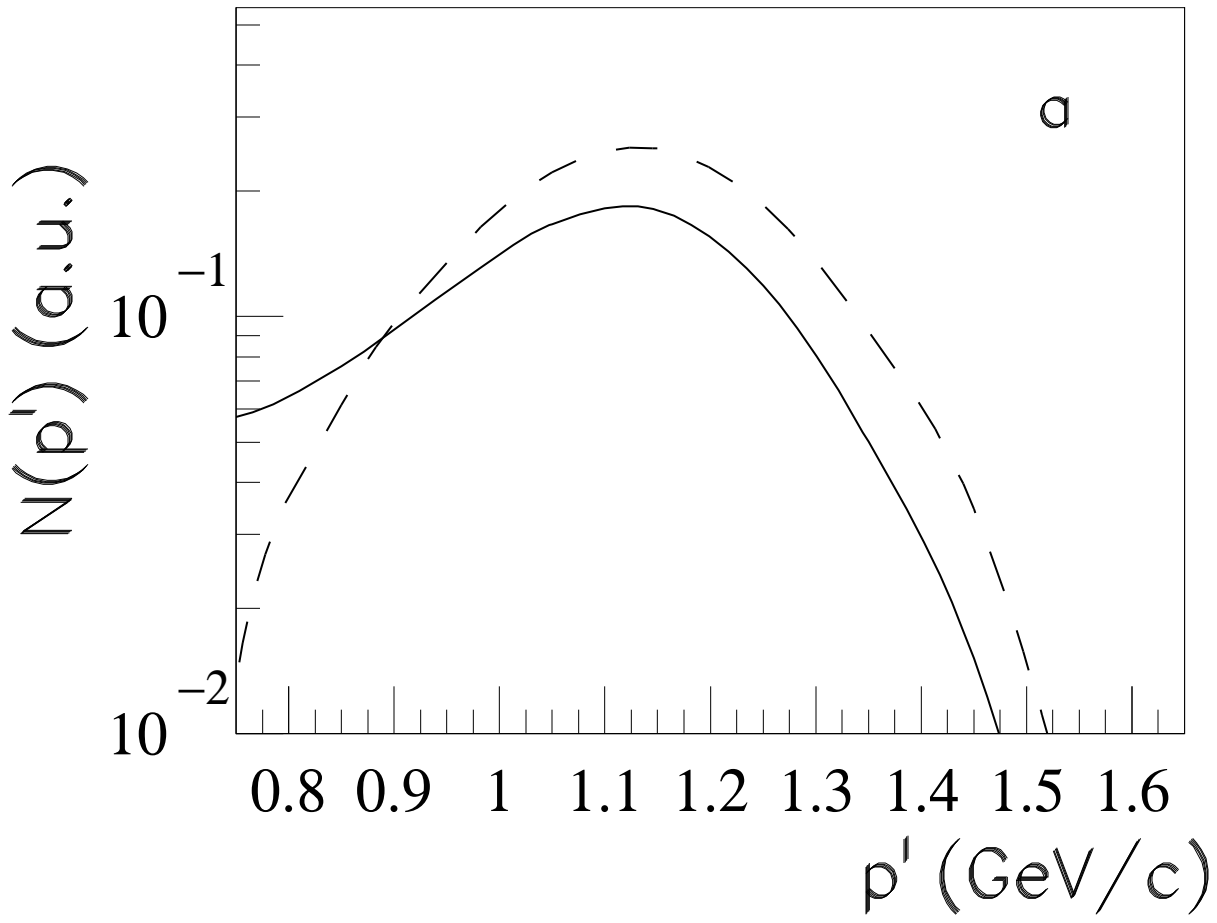


Fig. 4

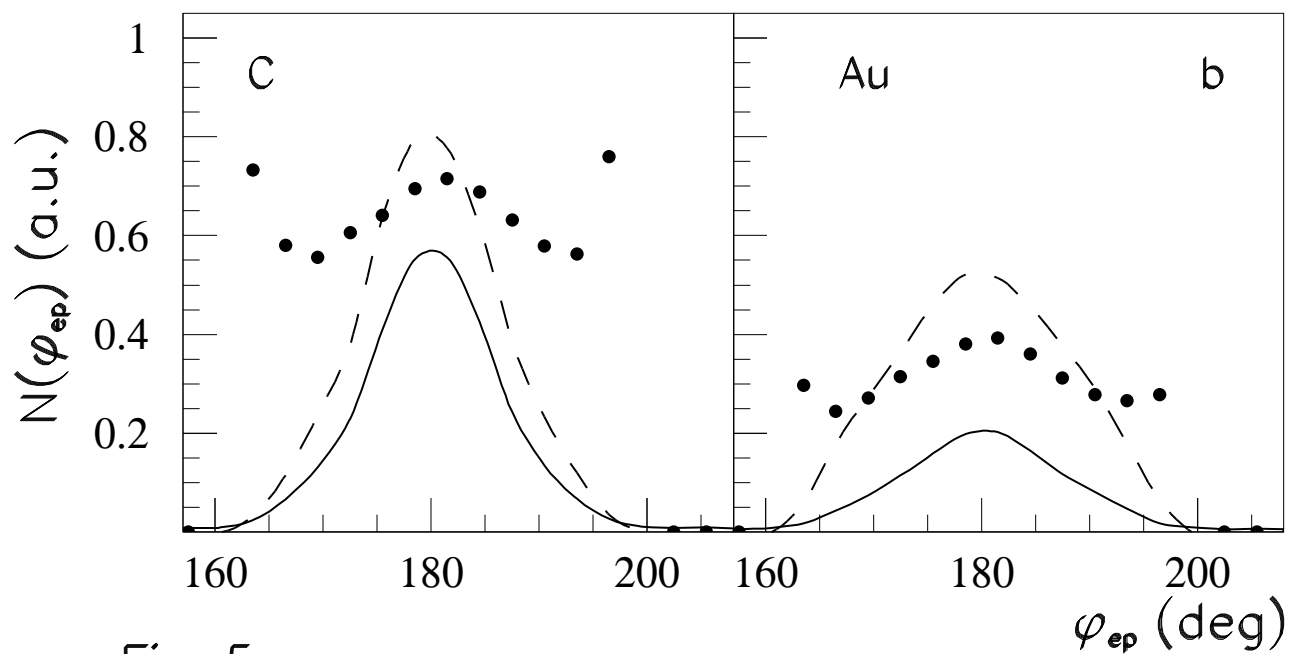
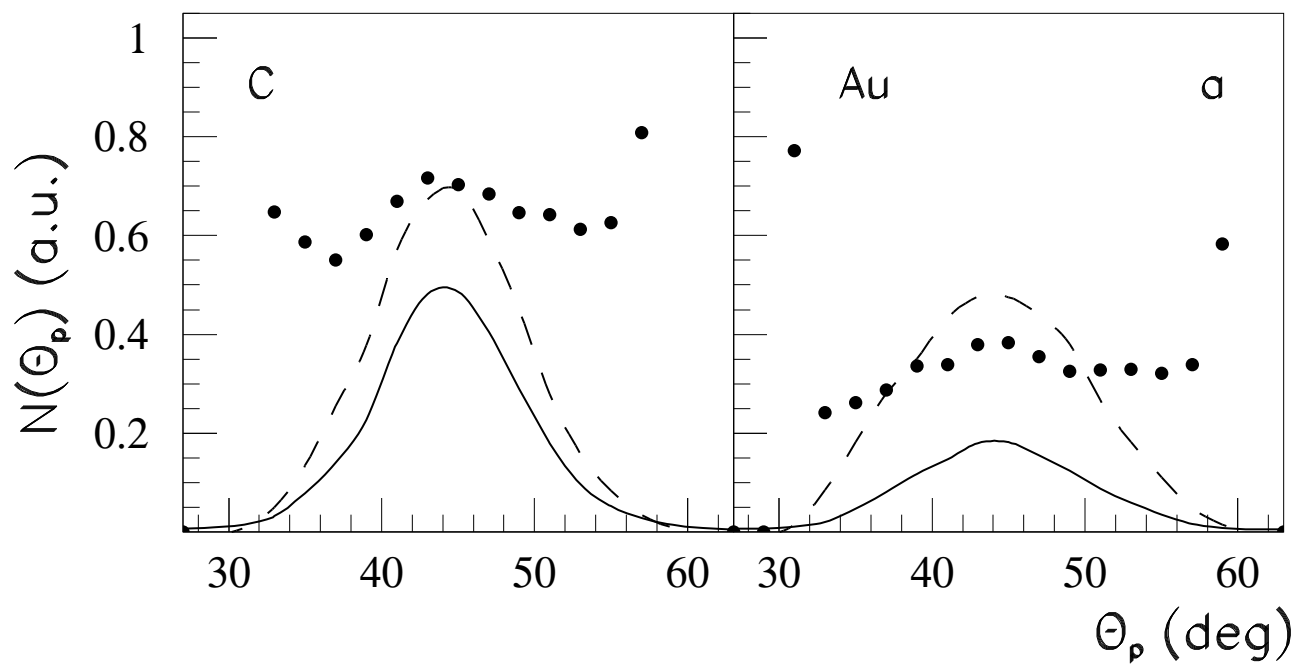


Fig. 5

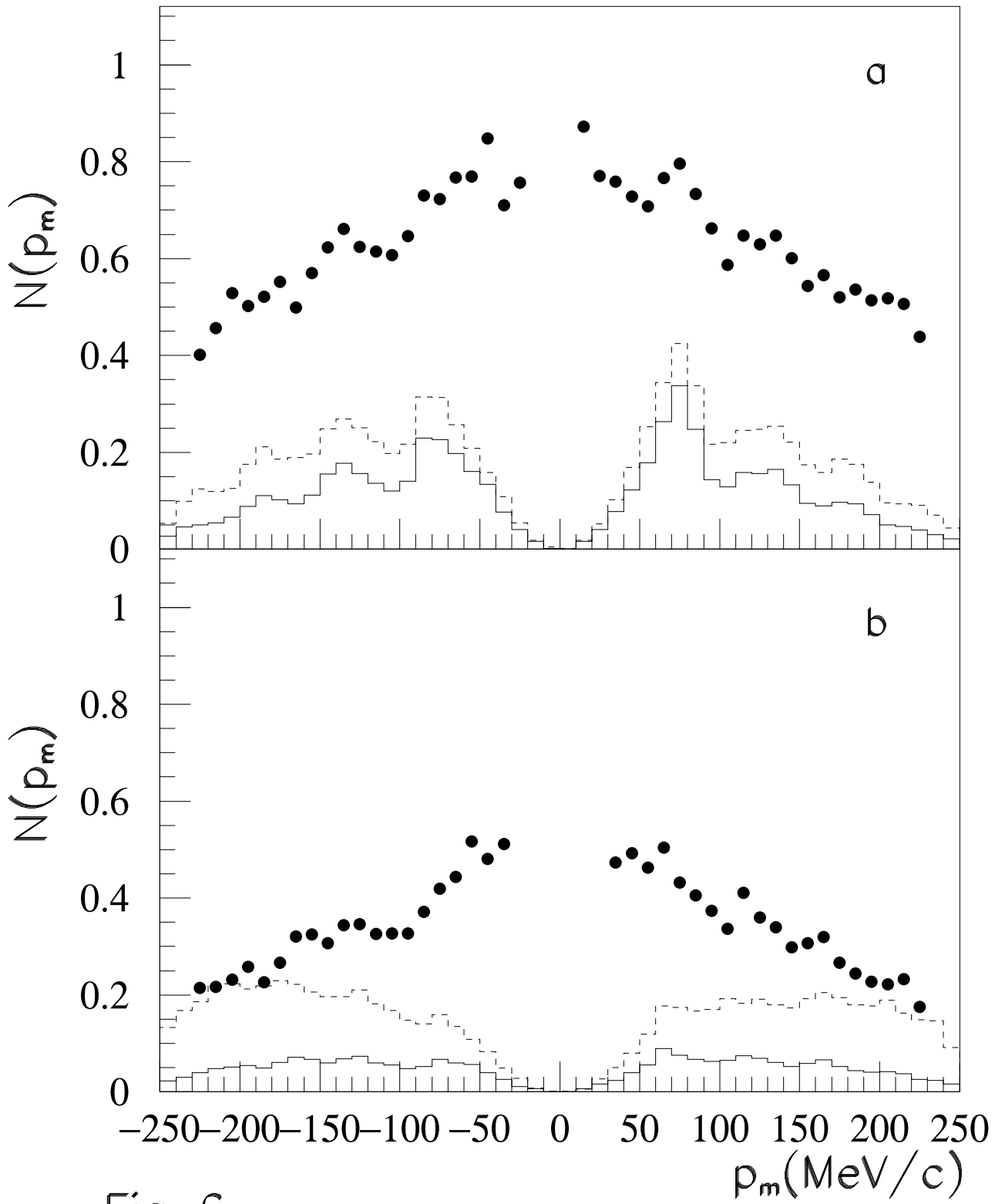


Fig. 6

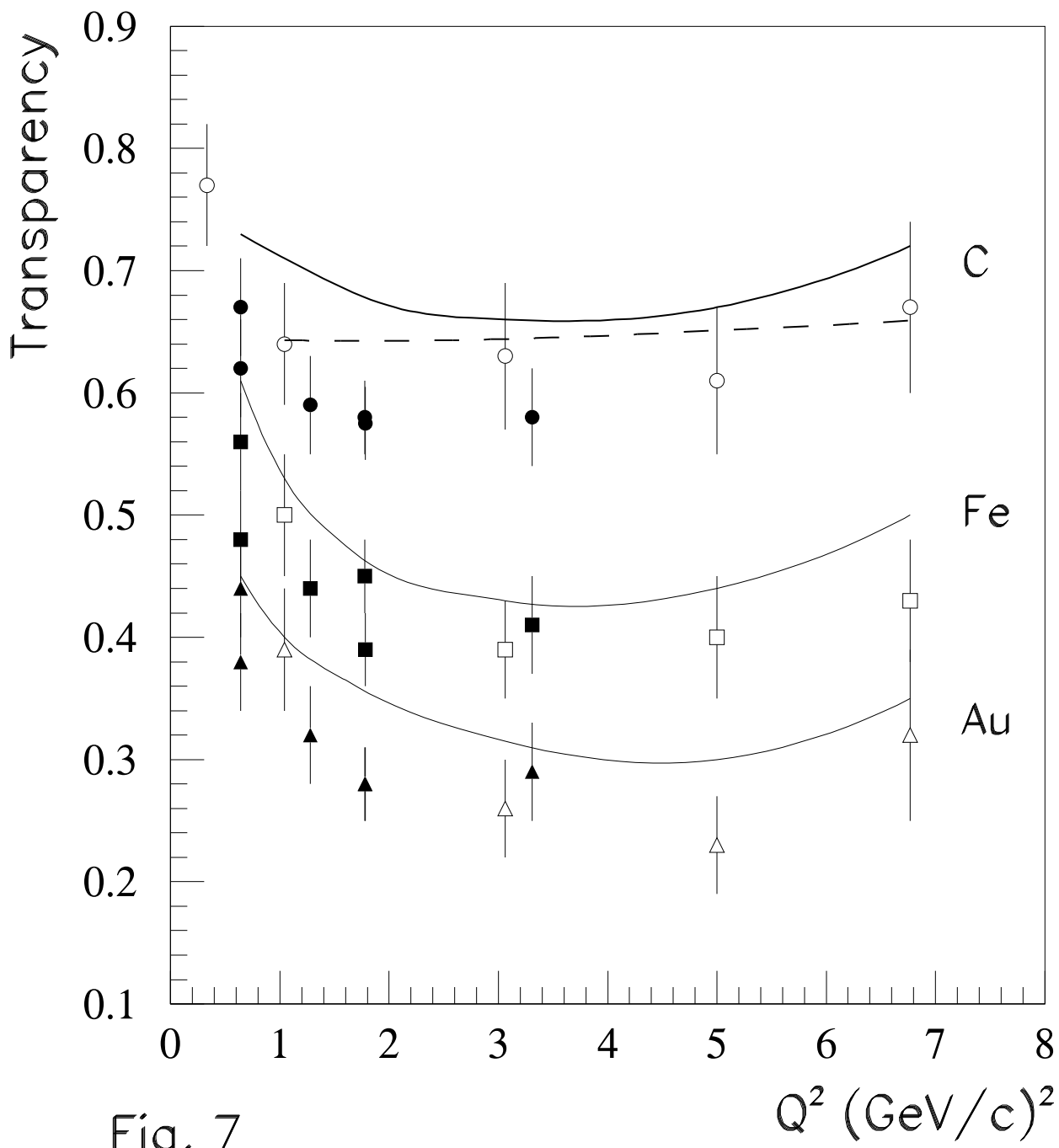


Fig. 7

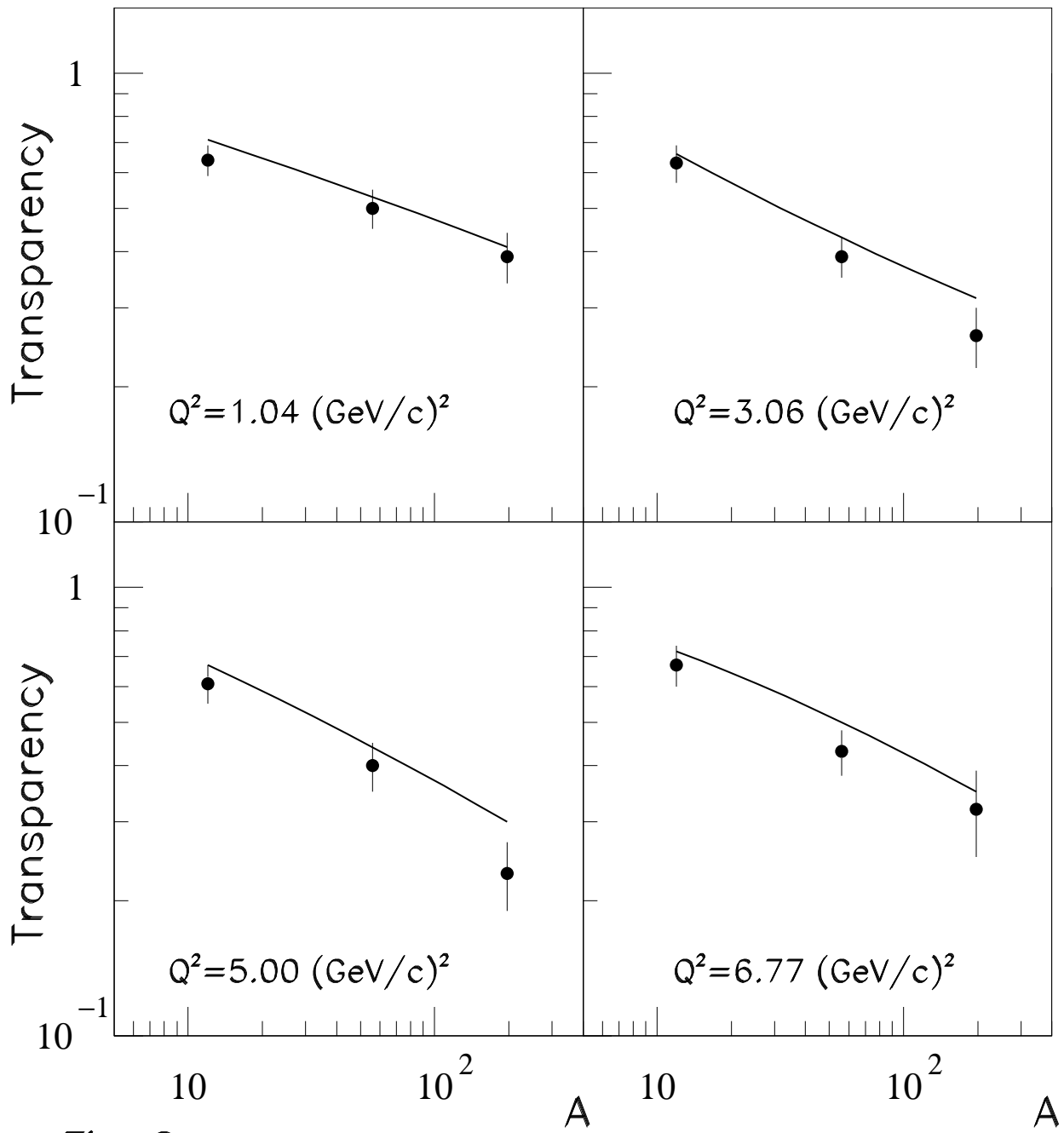


Fig. 8

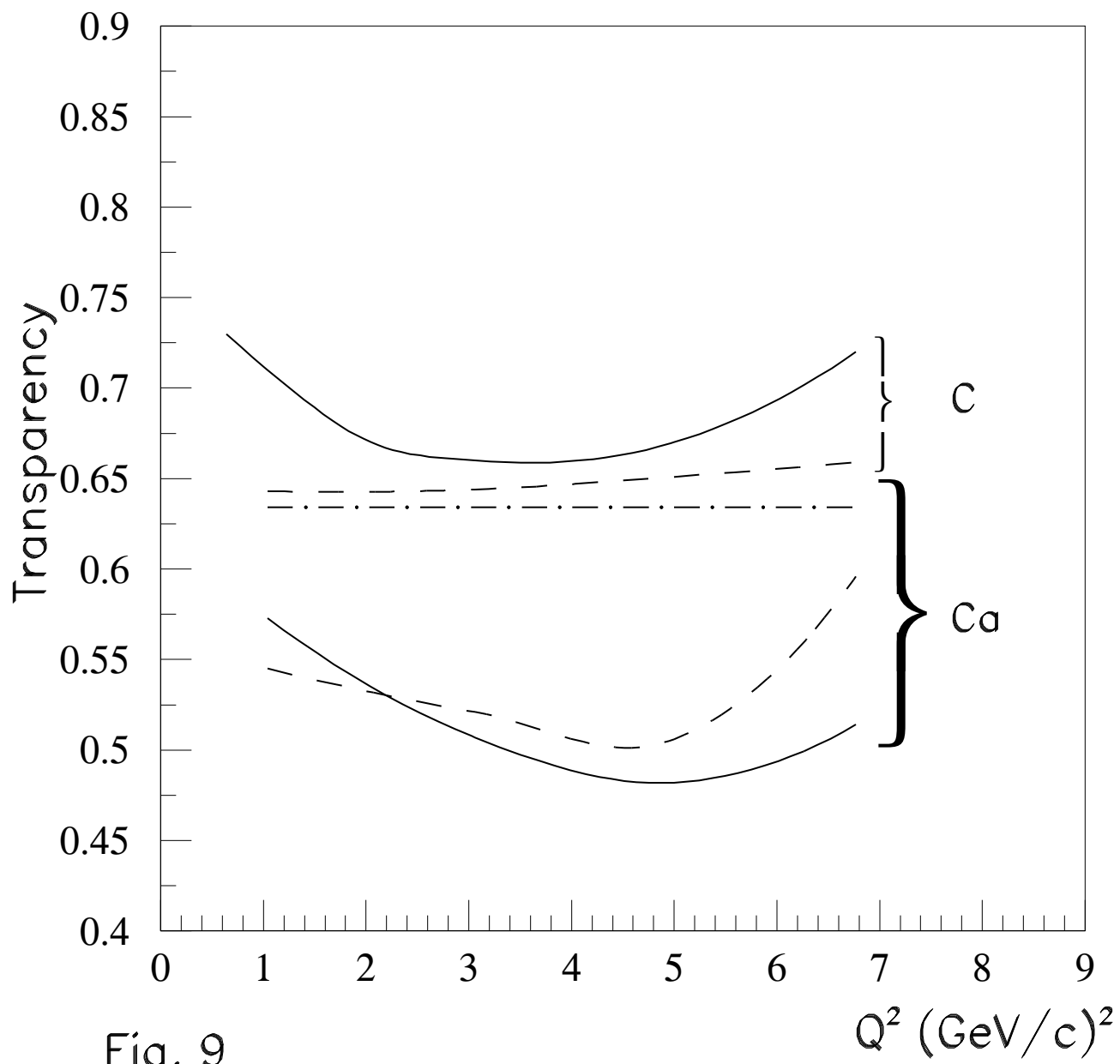


Fig. 9

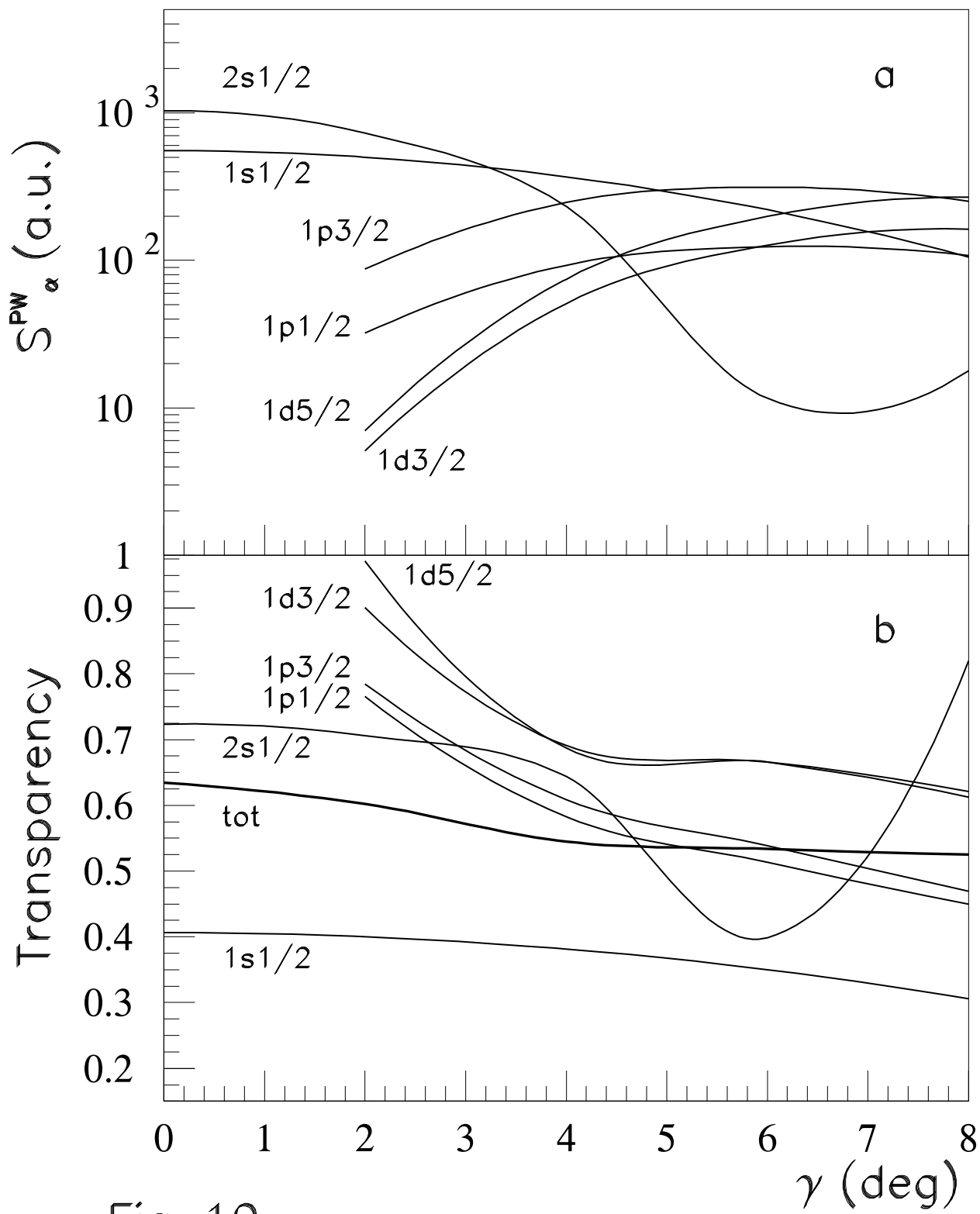


Fig. 10

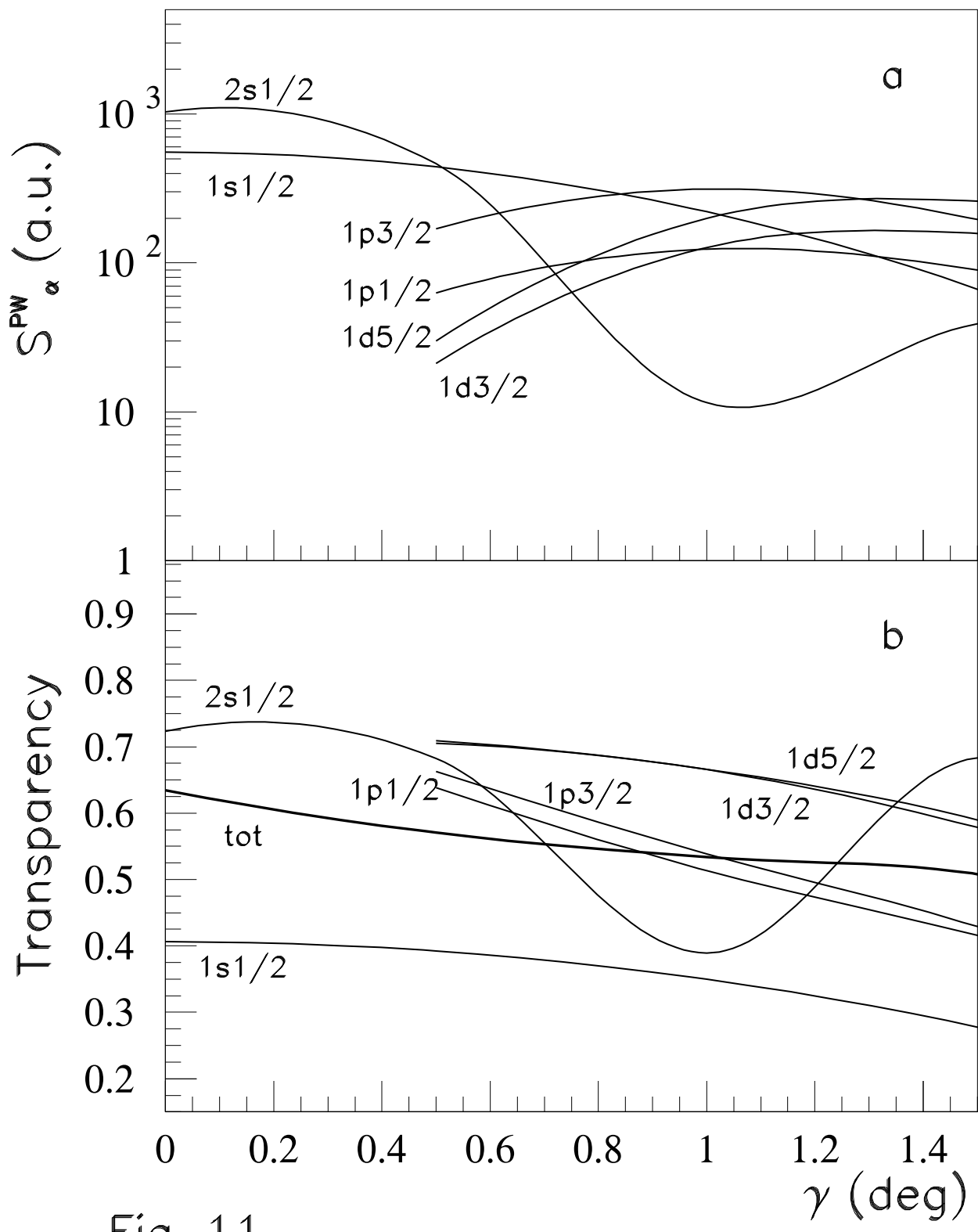


Fig. 11